

LETTER TO THE EDITOR

Spectral Evidence of Solar Neighborhood Analogs in CALIFA Galaxies

A. Mejía-Narváez¹, S. F. Sánchez¹, L. Carigi¹, J. K. Barrera-Ballesteros¹, N. Drory², and C. Espinosa-Ponce¹

¹ Instituto de Astronomía, Universidad Nacional Autónoma de México, A. P. 70-264, C.P. 04510, México, D.F., México

² McDonald Observatory, The University of Texas at Austin, 1 University Station, Austin, TX 78712, USA

Received September 15, 1996; accepted March 16, 1997

ABSTRACT

Aims. We introduce a novel non-parametric method to find solar neighborhood analogs (SNAs) in extragalactic IFS surveys. The main ansatz is that the physical properties of the solar neighborhood (SN) should be encoded in its optical stellar spectrum.

Methods. We assume that our best estimate of such spectrum is the one extracted from the analysis performed by the Code for Stellar properties Heuristic Assignment (CoSHA) from the MaStar stellar library. It follows that finding SNAs in other galaxies consist in matching, in a χ^2 sense, the SN reference spectrum across the optical extent of the observed galaxies. We apply this procedure to a selection of CALIFA galaxies, by requiring a close to face-on projection, relative isolation and non-AGN. We explore how the local and global properties of the SNAs (stellar age, metallicity, dust extinction, mass-to-light ratio, stellar surface mass and star-formation densities and galactocentric distance) and their corresponding host galaxies (morphological type, total stellar mass, star-formation rate, effective radius) compare with those of the SN and the Milky Way (MW).

Results. We find that SNAs are located preferentially in S(B)a – S(B)c galaxies, in a ring-like structure, which radii seems to scale with the galaxy size. Despite the known sources of systematics and errors, most properties present a considerable agreement with the literature on the SN. We conclude that the solar neighborhood is relatively common in our sample of SNAs. Our results warrants a systematic exploration of correlations among the physical properties of the SNAs and their host galaxies. We reckon that our method should inform current models of the galactic habitable zone in our MW and other galaxies.

Key words. Methods: statistical — Solar neighborhood — Galaxies stellar content

1. Introduction

Studies of the solar vicinity, whether such vicinity involves only a few hundreds of stars around the Sun or the whole Milky Way (MW), have the potential to answer fundamental questions about the formation of our galaxy and its satellites (e. g., Helmi et al. 2018; Ruiz-Lara et al. 2020), the formation of the Sun and its planets (e. g., Raymond et al. 2020) and ultimately the physical conditions needed to sustain life as we know it (e. g., Gonzalez et al. 2001). In an attempt to characterize the most likely zone in our MW with the conditions needed for life to sprout and thrive, Gonzalez et al. (2001) introduced the Galactic habitable zone (GHZ), a set of values for relevant physical properties that should constrain the habitability of different locations in the MW and in other galaxies. They suggested the GHZ as a ring-like structure located in the thin disk that extends with time toward the outskirts of the disk.

The GHZ was latter explored by Lineweaver et al. (2004). Based on chemical evolution models, those authors argued that the width of the ring should grow as a function of the cosmic time, due to the inside-out evolution of the disk (from 6 to 10 kpc). Similar results were found by Spitoni et al. (2014, 7 – 9 kpc). By considering the stellar density, Prantzos (2008) found that the most probable GHZ is in the inner disk (~ 3 kpc), later confirmed by Gowanlock et al. (2011). In the cosmological context, the GHZ has also been characterized through simulations, with the predictions that our Sun is not in the most probable GHZ, instead being either in the lower limit of the galactocentric distance distribution (e. g., Vukotić et al. 2016) or in the upper

limit (e. g., Forgan et al. 2017) and, more interestingly, not in the most likely host galaxy type (e. g., Zackrisson et al. 2016; Gobat & Hong 2016). Such theoretical results lack so far of a solid observational support.

The physical properties of the MW and the solar neighborhood (SN) have been widely studied in different surveys e. g., SEGUE (Yanny et al. 2009) APOGEE (Holtzman et al. 2015), GALAH (De Silva et al. 2015) and Gaia (Gaia Collaboration et al. 2018b). As a matter of fact, we have drawn a clear picture of our MW (see Bland-Hawthorn & Gerhard 2016, for a review; BH16 hereafter) and the SN (e. g., Buder et al. 2019), a knowledge that has been fed to simulations to reproduce observations with success (e. g., Prantzos et al. 2018). At global (i. e., the typical scale of a galaxy) and extragalactic scales, we have sampled hundreds of MW analogs in large surveys (e. g., Fraser-McKelvie et al. 2019; Boardman et al. 2020), leading to the conclusion that the MW is common among its analogs, but relatively rare among a complete sample of galaxies of the local Universe. At local scales (i. e., kpc scales and below), however, we have still to make progress in finding SN analogs (SNAs) in extragalactic surveys.

In this letter we seek to bridge the gap between simulations of the evolution of the SN and the whole MW, and current observations of its physical properties. Therefore, we use a non-parametric method to find SNAs in other galaxies that have been observed using Integral Field Unit (IFU). The main premise in our endeavor is that the physics of our SN is encoded in its integrated optical spectrum. Since we know for a fact that in our

SN life exists, it follows that the physical conditions defining our portion of the GHZ should also be encoded in such spectrum. We search for answers to the following questions: are SNAs properties, as found in other galaxies, similar to our own SN? will this rationale lead to the SN being a typical or an atypical environment in galaxies? in what type of galaxies – morphologically speaking – are SNAs more likely to be found? In particular we look for a characterization of the galactocentric distance distribution of the SNAs and to know if it scales with the host galaxy size. A natural follow up is to know if the Sun is in an expected location or if it is an outlier in this distribution. This letter is organized as follows: in § 2 we describe the samples and analysis methods; in § 3 we present our main findings; and finally we discuss and conclude in § 4.

2. Data and analysis

2.1. MaStar as a spectroscopic sample of solar neighborhood stars

MaStar (Yan et al. 2019) is a stellar library for the MaNGA survey (Bundy et al. 2015; Drory et al. 2015). Mejía-Narváez et al. (2021, hereafter MN21) labeled ~ 22 k unique stars in this library using CoSHA, a heuristic Machine Learning approach. One by-product of the analysis in MN21 that is relevant to the present letter is the partial volume correction implemented using the color-magnitude diagram (CMD) sampled by Gaia DR2 (Gaia Collaboration et al. 2018b). The Gaia survey has been implemented in the recent past to analyse the solar neighborhood properties (e. g., Ding et al. 2019; Sollima 2019; Gontcharov & Mosenkov 2021; Alzate et al. 2021), therefore it is a good survey to draw a photometric sample (e. g., Evans et al. 2018) of the solar surroundings. Knowing this, MN21 calculated a partial volume correction using the relation:

$$V_{\text{cor}} = \frac{\text{CMD}_{\text{MaStar}}}{\text{CMD}_{\text{Gaia}}}, \quad (1)$$

where $\text{CMD}_{\text{MaStar}}$ and CMD_{Gaia} represent the PDF distribution of stars in the extinction corrected CMD sampled by MaStar and Gaia (Gaia Collaboration et al. 2018a), respectively (e. g., Wall & Jenkins 2003; Rodríguez-Puebla et al. 2017; Sánchez et al. 2019). The “partial” character of this volume correction comes from the fact that Gaia is not a complete sample of the stars in the solar neighborhood. However it is, to our best knowledge, the most complete sample to date. The fact that the volume-corrected distributions of MaStar chemical abundances ($[\text{Fe}/\text{H}]$ and $[\alpha/\text{Fe}]$) resemble those from independent studies in the SN (c. f. Fig. 9 in MN21), is encouraging. Hence, we can assert that the *weighted averaged MaStar spectrum, with weights V_{cor} is, by design, our best estimate for the solar neighborhood optical spectrum*. In the following, we allude to this spectrum, f_{λ}^{SN} , as our spectroscopic reference of the solar neighborhood or simply the SN spectrum.

2.2. A solar neighborhood definition

The solar neighborhood is usually defined as the volume enclosed within a set radius around the Sun. There is no consensus, however, on the value of such radius and the literature on MW studies spans ranges from a few tens of pc to 1 kpc, depending on the specific subject of the research (e. g., Vergely et al. 1998; Aniyani et al. 2016). Here, we define the radial scale of the solar neighborhood *a posteriori*, as the standard deviation of

the volume corrected distance distribution of stars in the MaStar sample: $r_{\text{SN}} = 1.24$ kpc. This definition is consistent with the upper limit quoted above. It is also consistent with the typical physical resolution in the CALIFA sample, at the average redshift ~ 0.8 kpc (FWHM = $0.3 - 1.8$ kpc), which is indeed a convenient coincidence for the current study (although it does not impose a strong limitation). We note, that this definition is purely observational and that we may have a contribution from halo stars. However, as we will see below, any potential bias due to this selection should be accounted for by the projection effects of CALIFA galaxies.

2.3. A golden sample from CALIFA

CALIFA (Sánchez et al. 2012) is an integral field spectroscopic (IFS) survey of ~ 1000 galaxies in the nearby universe $z \sim 0.015$, complete to $M_{\star} \sim 10^{11.4} M_{\odot}$ and spanning all morphological types (Walcher et al. 2014; Galbany et al. 2018). We note that CALIFA is the only IFS survey that covers up to $2.5 r_{\text{eff}}$, i. e., most of the optical extension of galaxies is within the field-of-view (FoV) of the instrument, which is a relevant trait in our study (c. f. Table 1 in Sánchez 2020). The physical properties of these galaxies have been estimated and summarized using the Pipe3D pipeline (Sánchez et al. 2016a,b), which data-products have been extensively used in numerous publications (e. g., López-Cobá et al. 2020; Mejía-Narváez et al. 2020; Valerdi et al. 2021; Barrera-Ballesteros et al. 2021; Espinosa-Ponce et al. 2022). We focus our attention in galaxies that are not highly inclined in order to locate SNAs across their optical extent. In particular, we have three requirements for a galaxy to belong to our golden sample: (i) the inclination angle is ≤ 60 deg, also avoiding known issues (e. g., Ibarra-Medel et al. 2019), (ii) we have a reliable morphological classification; (iii) the galaxy has no evidence of nearby companions, ongoing collisions or post-merger signatures;¹ and (iv) the galaxy must not host an AGN according to Lacerda et al. (2020). After applying these constraints our initial sample is reduced to 330 galaxies, ($\sim 1/3$) of the original CALIFA sample. This golden selection poses the possibility of finding SNAs in galaxies that hold no *a priori* resemblance with the MW.

2.4. Finding solar neighborhood analogs

We look for the SNA across the optical extent of CALIFA galaxies by exploring the spatial distribution of the χ^2 , in which the observed spectra in each spaxel is compared with our reference spectrum for the SN in the MW (§ 2.2). For this purpose, the SN reference spectrum is convolved with a Gaussian function and dust attenuated using the Cardelli et al. (1989) model, following the procedures in pyFIT3D (Lacerda et al. 2022, Eq. 1). Hence, we account for (1) the redshift and velocity rotation of the galaxy, (2) the line-of-sight velocity dispersion, and (3) the differential extinction due to projection and line-of-sight effects. To further account for the differential physical spatial resolution of each spaxel ($\sim 1''$) at the observed galaxy redshift, the CALIFA cubes are convolved with a Gaussian kernel to match the resolution of our SN region (~ 1 kpc, § 2.2).

Based on the χ^2 -matching we perform for each spaxel, we label as SNA those regions in which the χ^2_{ij} is within the range $0.7 - 1.3$, avoiding at the same time, the spaxels that mismatch with our reference spectrum (> 1.3) and those with over estimated uncertainties (< 0.7).

¹ We will analyze interacting galaxies in a another paper.

3. Results

Fig. 1 summarizes our main results for three galaxies hosting SNA regions, as an illustrative example: NGC 5947, NGC 5000 and NGC 309. For each galaxy we show the contour of the likelihood map ($\mathcal{L}_{ij} \propto \exp[-\chi^2_{ij}/2]$) on top of the RGB composite image, highlighting the location of the most likely SNA. In addition we show the corresponding spectra of those regions together with the reference SNA spectrum. We observe that the SNA spectrum of the three example galaxies is well within the uncertainty band, σ_λ (shaded region), for most of the wavelength range. A higher \mathcal{L}_{SNA} indicates that the likelihood of finding a SNA within the target galaxy is more concentrated around a specific region. In top panels of Fig. 1, NGC 5000 shows the most concentrated likelihood of hosting SNA spaxels, with an apparent azimuthal symmetry. At first sight, this pattern is also followed by NGC 5947 and NGC 309, whereby likely SNA spaxels group in a ring-like structure. Interestingly, the radius of such structure seems to depend on the galaxy's apparent size. We will explore this below.

Repeating the above analysis for each galaxy we find SNAs in only 61 out of 330 galaxies ($\sim 20\%$). Table 1 shows the physical properties of the MW and in our solar vicinity (column 2) together with those of the host galaxies and the corresponding most likely SNA regions (column 3). A detailed exploration of these properties will be presented in a forthcoming study. We present here a brief summary of such exploration.

Despite remaining agnostic about the global and local physical properties of potential host galaxies, we find that *most* likely SNA regions (within 1σ) are more frequent in spiral galaxies ranging Sa – Sc and that these regions seem to lie preferentially in between arms. As a matter of fact, this is the expectation in the MW (Sb – Sbc), where the Sun is known to be located between Perseus and Carina-Sagittarius arms (e. g., BH16). The median global stellar mass (Fig. 2a), $\log M_\star/M_\odot \sim 10.91 \pm 0.26$ and star-formation rate (SFR; Fig. 2b), $\log \psi_\star \sim 0.46 \pm 0.43 \text{ M}_\odot \text{ yr}^{-1}$, for our sample of host galaxies, is also consistent with reported values for the MW (e. g., Fraser-McKelvie et al. 2019). However, we note that the corresponding MW values are within 1σ of the host galaxies sample, closer to its lower limit (c. f., Table 1). We know that most global properties of galaxies scale with its size (e. g., Sánchez et al. 2021, and references therein), therefore we also compare the median effective radius of the host galaxies sample, $r_{\text{eff}} \sim 5.76 \pm 3.32 \text{ kpc}$ to the Galaxy value. Given the location of the Sun within the MW disk, a precise measure of its radial scale-length is difficult (see, BH16, for a review). We assume the reviewed radial scale-length $\sim 2.5 \pm 0.4 \text{ kpc}$. To convert to effective radius we multiply by 1.68 (Sánchez et al. 2014), resulting in an estimated effective radius for the MW of $r_{\text{eff}} \sim 4.2 \pm 0.4 \text{ kpc}$. As in the case of the stellar mass and the SFR, the MW lies within 1σ of the distribution of SNA host galaxies, with the latter ones being systematically larger than the MW. These values of global properties suggest that SNA are more likely to thrive in galaxies that meet well defined physical conditions.

Even though the global properties explored above have restricted the type of galaxies in which SNA are likely to be found, local properties have the potential to unveil the environmental physics of such regions. The local conditions of the SN have been widely studied in recent years and we have revealed a clear picture of our vicinity through a wide variety of stellar tracers (e. g., Bonatto & Bica 2011; Sollima 2019; Şahin & Bilir 2020; Whitten et al. 2021; Gontcharov & Mosenkov 2021, to name a few). The SN is known to be in an expanding local under-

Table 1. Median global and local properties for the MW and the SN, respectively, compared to the SNA hosts and regions values retrieved in this letter.

	MW/SN	CALIFA/SNA
Global		
Type	S(B)b – bc	S(B)a – c
$\log M_\star/M_\odot$	10.70 ± 0.09	10.95 ± 0.26
$\log \psi_\star$	0.22 ± 0.05	0.41 ± 0.43
r_{eff}	4.20 ± 0.40	5.18 ± 3.32
Local		
$\langle \log t/\text{yr} \rangle_{L_\star}$	9.38 ± 0.09	9.10 ± 0.17
$\langle \log t/\text{yr} \rangle_{M_\star}$	9.70 ± 0.22	9.76 ± 0.14
$\langle [Z/Z_\odot] \rangle_{L_\star}$	-0.08 ± 0.18	-0.20 ± 0.09
$\langle [Z/Z_\odot] \rangle_{M_\star}$	-0.06 ± 0.20	-0.17 ± 0.14
A_V	0.19 ± 0.02	0.15 ± 0.25
$\log M_\star/L_\star$	0.36 ± 0.04	0.60 ± 0.12
$\log \Sigma_{M_\star}$	1.76 ± 0.07	1.85 ± 0.27
$\log \Sigma_{\psi_\star}$	-8.24 ± 0.09	-8.44 ± 0.50
$r_{\text{SNA}}/r_{\text{eff}}$	1.95 ± 0.19	2.05 ± 1.61

density called the local bubble ($< 200 \text{ pc}$) with little to none star formation within (e. g., Zucker et al. 2022), low dust extinction (e. g., Gaia Collaboration et al. 2018a), stellar metallicity around solar value (e. g., Hayden et al. 2020) and an average (mass-weighted) stellar age $\langle \log t/\text{yr} \rangle_{M_\star} \sim 9.5$ (e. g., Reid et al. 2007). Outside this vicinity ($< 1 \text{ kpc}$) the solar neighborhood star formation takes place at a rate per square parsec of $\log \Sigma_{\psi_\star} \sim -8.24 \pm 0.09 \text{ M}_\odot \text{ yr}^{-1} \text{ pc}^{-2}$; this yields a light dominant stellar component with age $\langle \log t/\text{yr} \rangle_{L_\star} \lesssim 9.38 \pm 0.09$ and metallicity $\langle [Z/Z_\odot] \rangle_{L_\star} \lesssim -0.08 \pm 0.18$ (Fig. 2c); with a surface mass density $\log \Sigma_{M_\star} \sim 1.76 \pm 0.07 \text{ M}_\odot \text{ pc}^{-2}$ and mass-to-light ratio in the V-band $\log M_\star/L_\star \sim 0.36 \pm 0.04 \text{ M}_\odot L_\odot^{-1}$ (Flynn et al. 2006) and; affected by a typical visual dust extinction $A_V \sim 0.19 \pm 0.02 \text{ mag}$.

In most of the cases we find an astonishing agreement in their local properties, despite of the different methodologies adopted to derive the SNA values (stellar population synthesis of unresolved stars), and the SN ones (exploring the properties of resolved stellar populations; see e. g., Reid et al. 2007; Hayden et al. 2020; Gontcharov & Mosenkov 2021; Lacerda et al. 2022). Of the compared properties we found difference above 2σ for only the M_\star/L_\star ratio, a parameter that is particularly difficult to derive for resolved stellar populations (e. g., Flynn et al. 2006).

As indicated before we find that most of the SNA regions are located following a ring-like distribution around the galactic nucleus (e. g., Fig. 1). This ring seems to be located at different galactocentric distances for each galaxy, as suggested by Prantzos (2008) for the MW. We noted above that this distance seemingly scales with the size of the galaxy. In order to check for this possibility, we present in Fig. 2d the distribution of the galactocentric distances for the SNAs normalized by the effective radius of the host galaxy. The fact that the SNA distances distribution can be characterized by a typical value is evidence that such regions tend to thrive around a typical scaled radii value, albeit with a significant scatter, $\sigma_{r_{\text{SNA}}} \sim 1.79 r_{\text{eff}}$. According to our estimates of the MW effective radius, the SN is located at a scaled galactocentric distance of $r_{\text{SN}} \sim 1.95 \pm 0.19 r_{\text{eff}}$, assuming a Sun absolute galactocentric distance $\sim 8.2 \pm 0.1 \text{ kpc}$ (BH16). Interestingly, the median distance of SNAs and that of the Sun are ~ 2 , and are apart by $\sim 0.1 r_{\text{eff}}$.

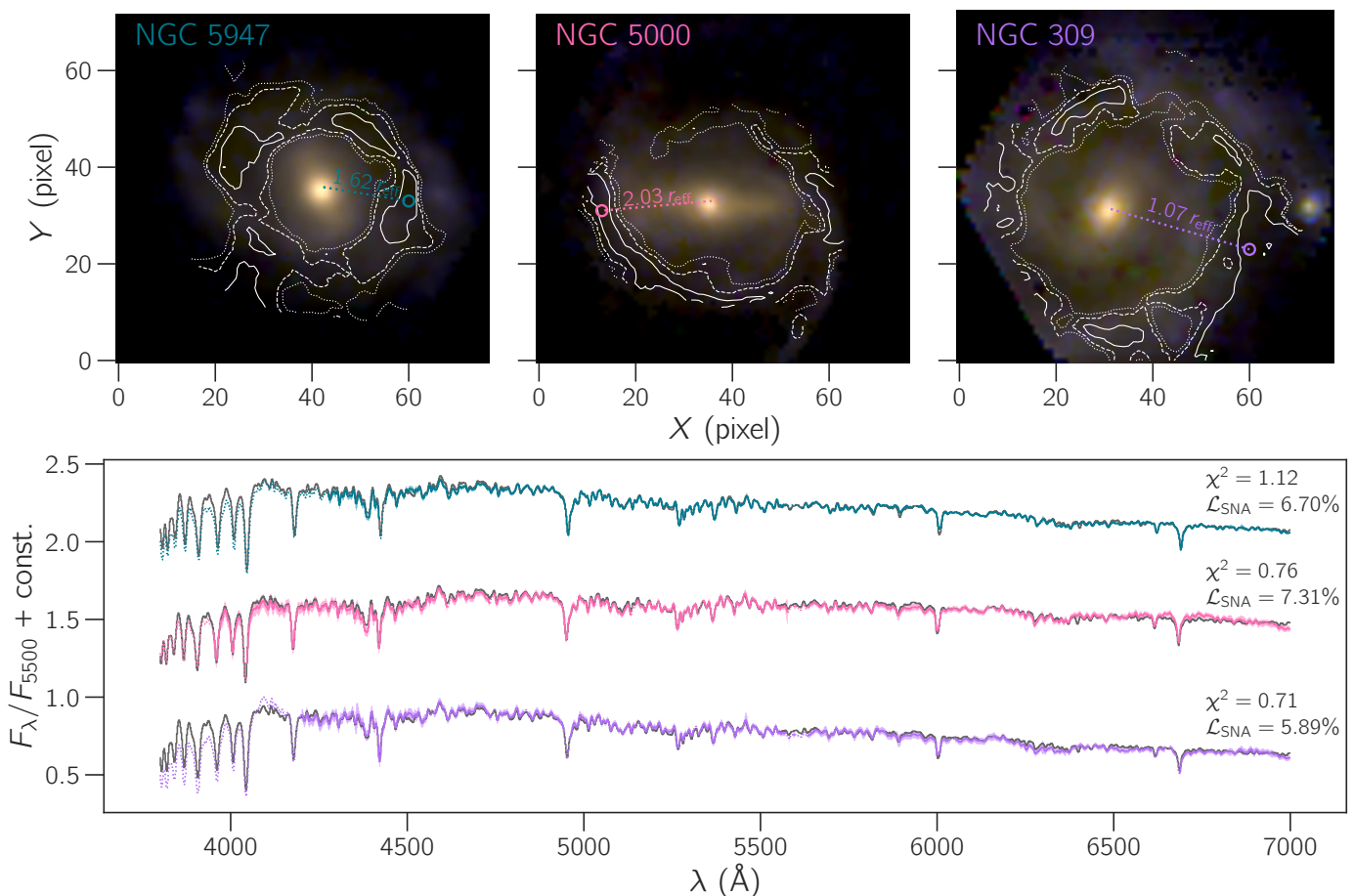


Fig. 1. *Top panels:* The RGB (R: 6450 Å, G: 5375 Å and B: 3835 Å) composite images of galaxies NGC 5947, NGC 5000 and NGC 309 in our golden sample described in § 2.3 that host likely SNA regions. The likelihood map is overlaid in each case with contours enclosing the 1σ (solid), 2σ (dashed) and 3σ (dotted), respectively. The location of the maximum likelihood in each case (colored circle) and its galactocentric distance (dashed colored line) are shown. *Bottom panel:* the spectrum corresponding to the maximum likelihood spaxel (solid line in color) along with the propagated (1σ) error spectrum is also shown as a shaded region. We highlight the regions where the error spectrum was masked out (dotted). The SNA spectrum (gray) calculated as described in § 2.4 is also shown. The resulting χ^2 and the likelihood integrated within r_{pix} around the maximum are also shown.

4. Discussion and conclusions

Most of the efforts to characterize the GHZ in the MW are based on simulations of galaxy formation and chemical evolution. Lineweaver et al. (2004) simulated the physical conditions to produce a MW-like galaxy. They predicted that the Sun lies well within a locus of GHZ, which encompasses a stellar population with an age $\lesssim 4 - 8$ Gyr ($\log t/\text{yr} \lesssim 9.6 - 9.9$) and galactocentric distances within $\sim 5 - 11$ kpc ($1.19 - 2.62 r_{\text{eff}}$). Spitoni et al. (2014, 2017) developed chemical evolution simulations of the MW and M31 to predict the probability of finding terrestrial planets with the conditions to harbor life. In agreement with Lineweaver et al. (2004), they also found that earth-like planets are more likely in the present than in the past, peaking near 8 kpc in galactocentric distance. Interestingly, Spitoni et al. (2014) finds for M31 that earth-like planets are prone to be found at systematically larger galactocentric radii ~ 16 kpc. Similarly, Carigi et al. (2013) found $\sim 12 - 14$ kpc for the same galaxy. Assuming a $r_{\text{eff}} \sim 9$ kpc for M31, these radii are within 1σ of our distribution in Fig. 2d. These results are also consistent with earlier characterizations of the GHZ in our galaxy made by Lineweaver et al. (2004); Prantzos (2008). They argued that, as the Galactic disk evolves inside-out, the ring-shaped GHZ spreads toward inner and outer regions of the MW. The pic-

ture drawn from these simulations is consistent with our findings that the SNAs in galaxies other than the MW follow a ring-like structure, which radii depends on the size of the galaxy. Consequently, the GHZ (as sampled by our SN definition) should be related to the time-scale at which these galaxies are currently evolving, as gathered from their current total stellar mass and metallicity, SFR, etc.

In summary, the newly introduced methodology has allowed us to find SNAs using a non-parametric method. Most of the local properties of those regions and the global ones of their hosts agree with the those of the SN and the MW. Furthermore, SNAs are found in a ring at a galactocentric distance that scales with the size of the galaxy. This result agrees with both our current understanding of the evolution of the stellar populations in galaxies (e. g., Sánchez 2020) and simulations predicting the optical location of both the GHZ and the presence of terrestrial planets. A study of the structural evolution of these potential GHZs at higher redshifts is in order.

Acknowledgements. We thank the support by the PAPIIT-DGAPA grant AG100622. AMN thanks the support from the DGAPA-UNAM postdoctoral fellowship. LC thanks support from (PAPIIT-DGAPA, UNAM), grant IN-103820. JBB acknowledges support from the grant IA-101522 (PAPIIT-DGAPA, UNAM) and funding from the CONACYT grant CF19-39578. We thank the anonymous referee for his/her helpful comments. This study makes uses of

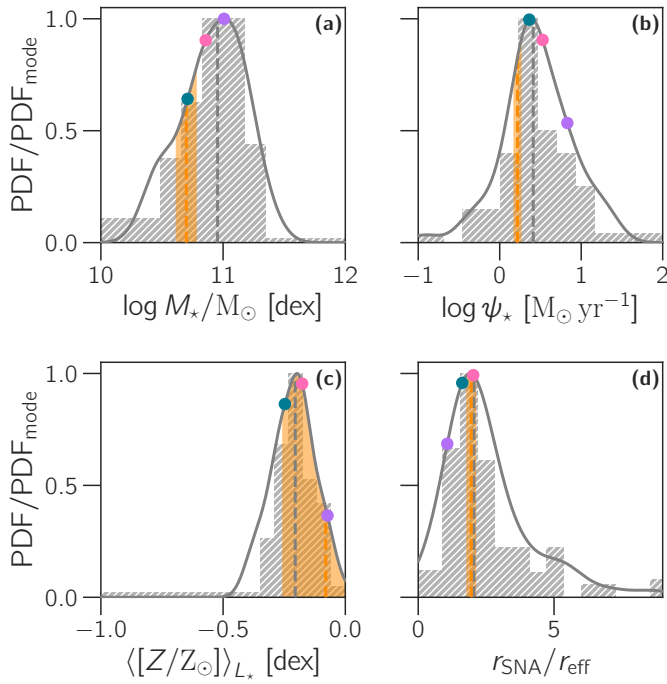


Fig. 2. Distributions of global (a) stellar mass and (b) SFR; and local (c) luminosity-weighted stellar metallicity and (d) galactocentric distances normalized by the host effective radius, for the 61 host and SNAs (gray shaded histogram and density plot), respectively. The corresponding median of each distribution is shown (gray dashed line). The 3 example galaxies from Fig. 1 are also highlighted (circles). The vertical orange region indicates the galactocentric distance of the Sun with respect to the r_{eff} of the MW ($\pm 1\sigma$) around the best estimate (orange dashed line).

the data provided by the Calar Alto Legacy Integral Field Area (CALIFA) survey (<http://califa.caha.es>). CALIFA is the first legacy survey being performed at Calar Alto. The CALIFA collaboration would like to thank the IAA-CSIC and MPIA-MPG as major partners of the observatory, and CAHA itself, for the unique access to telescope time and support in manpower and infrastructures. The CALIFA collaboration thanks also the CAHA staff for the dedication to this project. Funding for the Sloan Digital Sky Survey IV has been provided by the Alfred P. Sloan Foundation, the U.S. Department of Energy Office of Science, and the Participating Institutions. SDSS-IV acknowledges support and resources from the Center for High Performance Computing at the University of Utah. The SDSS website is www.sdss.org. SDSS-IV is managed by the Astrophysical Research Consortium for the Participating Institutions of the SDSS Collaboration including the Brazilian Participation Group, the Carnegie Institution for Science, Carnegie Mellon University, Center for Astrophysics | Harvard & Smithsonian, the Chilean Participation Group, the French Participation Group, Instituto de Astrofísica de Canarias, The Johns Hopkins University, Kavli Institute for the Physics and Mathematics of the Universe (IPMU) / University of Tokyo, the Korean Participation Group, Lawrence Berkeley National Laboratory, Leibniz Institut für Astrophysik Potsdam (AIP), Max-Planck-Institut für Astronomie (MPIA Heidelberg), Max-Planck-Institut für Astrophysik (MPA Garching), Max-Planck-Institut für Extraterrestrische Physik (MPE), National Astronomical Observatories of China, New Mexico State University, New York University, University of Notre Dame, Observatório Nacional / MCTI, The Ohio State University, Pennsylvania State University, Shanghai Astronomical Observatory, United Kingdom Participation Group, Universidad Nacional Autónoma de México, University of Arizona, University of Colorado Boulder, University of Oxford, University of Portsmouth, University of Utah, University of Virginia, University of Washington, University of Wisconsin, Vanderbilt University, and Yale University.

References

Alzate, J. A., Bruzual, G., & Díaz-González, D. J. 2021, *MNRAS*, 501, 302
 Aniyani, S., Freeman, K. C., Gerhard, O. E., Arnaboldi, M., & Flynn, C. 2016, *MNRAS*, 456, 1484

Barrera-Ballesteros, J. K., Heckman, T., Sánchez, S. F., et al. 2021, *ApJ*, 909, 131
 Bland-Hawthorn, J. & Gerhard, O. 2016, *ARA&A*, 54, 529
 Boardman, N., Zasowski, G., Seth, A., et al. 2020, *MNRAS*, 491, 3672
 Bonatto, C. & Bica, E. 2011, *MNRAS*, 415, 2827
 Buder, S., Lind, K., Ness, M. K., et al. 2019, *A&A*, 624, A19
 Bundy, K., Bershad, M. A., Law, D. R., et al. 2015, *ApJ*, 798, 7
 Cardelli, J. A., Clayton, G. C., & Mathis, J. S. 1989, *ApJ*, 345, 245
 Carigi, L., García-Rojas, J., & Meneses-Goytia, S. 2013, *Rev. Mexicana Astron. Astrofis.*, 49, 253
 Şahin, T. & Bilir, S. 2020, *ApJ*, 899, 41
 De Silva, G. M., Freeman, K. C., Bland-Hawthorn, J., et al. 2015, *MNRAS*, 449, 2604
 Ding, P. J., Zhu, Z., & Liu, J. C. 2019, *AJ*, 158, 247
 Drory, N., MacDonald, N., Bershad, M. A., et al. 2015, *AJ*, 149, 77
 Espinosa-Ponce, C., Sánchez, S. F., Morisset, C., et al. 2022, *MNRAS*, 512, 3436
 Evans, D. W., Riello, M., De Angeli, F., et al. 2018, *A&A*, 616, A4
 Flynn, C., Holmberg, J., Portinari, L., Fuchs, B., & Jahreiß, H. 2006, *MNRAS*, 372, 1149
 Forgan, D., Dayal, P., Cockell, C., & Libeskind, N. 2017, *International Journal of Astrobiology*, 16, 60
 Fraser-McKelvie, A., Merrifield, M., & Aragón-Salamanca, A. 2019, *MNRAS*, 489, 5030
 Gaia Collaboration, Babusiaux, C., van Leeuwen, F., et al. 2018a, *A&A*, 616, A10
 Gaia Collaboration, Brown, A. G. A., Vallenari, A., et al. 2018b, *A&A*, 616, A1
 Galbany, L., Anderson, J. P., Sánchez, S. F., et al. 2018, *ApJ*, 855, 107
 Gobat, R. & Hong, S. E. 2016, *A&A*, 592, A96
 Gontcharov, G. A. & Mosenkov, A. V. 2021, *MNRAS*, 500, 2590
 Gonzalez, G., Brownlee, D., & Ward, P. 2001, *Icarus*, 152, 185
 Gowanlock, M. G., Patton, D. R., & McConnell, S. M. 2011, *Astrobiology*, 11, 855
 Hayden, M. R., Bland-Hawthorn, J., Sharma, S., et al. 2020, *MNRAS*, 493, 2952
 Helmi, A., Babusiaux, C., Koppelman, H. H., et al. 2018, *Nature*, 563, 85
 Holtzman, J. A., Shetrone, M., Johnson, J. A., et al. 2015, *AJ*, 150, 148
 Ibarra-Medel, H. J., Avila-Reese, V., Sánchez, S. F., González-Samaniego, A., & Rodríguez-Puebla, A. 2019, *MNRAS*, 483, 4525
 Lacerda, E. A. D., Sánchez, S. F., Cid Fernandes, R., et al. 2020, *MNRAS*, 492, 3073
 Lacerda, E. A. D., Sánchez, S. F., Mejía-Narváez, A., et al. 2022, *arXiv e-prints*, arXiv:2202.08027
 Lineweaver, C. H., Fenner, Y., & Gibson, B. K. 2004, *Science*, 303, 59
 López-Cobá, C., Sánchez, S. F., Anderson, J. P., et al. 2020, *AJ*, 159, 167
 Mejía-Narváez, A., Bruzual, G., Sánchez, S. F., et al. 2021, *arXiv e-prints*, arXiv:2108.01697
 Mejía-Narváez, A., Sánchez, S. F., Lacerda, E. A. D., et al. 2020, *MNRAS*, 499, 4838
 Prantzos, N. 2008, *Space Sci. Rev.*, 135, 313
 Prantzos, N., Abia, C., Limongi, M., Chieffi, A., & Cristallo, S. 2018, *MNRAS*, 476, 3432
 Raymond, S. N., Izidoro, A., & Morbidelli, A. 2020, in *Planetary Astrobiology*, ed. V. S. Meadows, G. N. Arney, B. E. Schmidt, & D. J. Des Marais, 287
 Reid, I. N., Turner, E. L., Turnbull, M. C., Mountain, M., & Valenti, J. A. 2007, *ApJ*, 665, 767
 Rodríguez-Puebla, A., Primack, J. R., Avila-Reese, V., & Faber, S. M. 2017, *MNRAS*, 470, 651
 Ruiz-Lara, T., Gallart, C., Bernard, E. J., & Cassisi, S. 2020, *Nature Astronomy*, 4, 965
 Sánchez, S. F. 2020, *ARA&A*, 58, 99
 Sánchez, S. F., Avila-Reese, V., Rodríguez-Puebla, A., et al. 2019, *MNRAS*, 482, 1557
 Sánchez, S. F., Kennicutt, R. C., Gil de Paz, A., et al. 2012, *A&A*, 538, A8
 Sánchez, S. F., Pérez, E., Sánchez-Blázquez, P., et al. 2016a, *Rev. Mexicana Astron. Astrofis.*, 52, 171
 Sánchez, S. F., Pérez, E., Sánchez-Blázquez, P., et al. 2016b, *Rev. Mexicana Astron. Astrofis.*, 52, 21
 Sánchez, S. F., Rosales-Ortega, F. F., Iglesias-Páramo, J., et al. 2014, *A&A*, 563, A49
 Sánchez, S. F., Walcher, C. J., Lopez-Cobá, C., et al. 2021, *Rev. Mexicana Astron. Astrofis.*, 57, 3
 Sollima, A. 2019, *MNRAS*, 489, 2377
 Spitoni, E., Giovannini, L., & Matteucci, F. 2017, *A&A*, 605, A38
 Spitoni, E., Matteucci, F., & Sozzetti, A. 2014, *MNRAS*, 440, 2588
 Valerdi, M., Barrera-Ballesteros, J. K., Sánchez, S. F., et al. 2021, *MNRAS*, 505, 5460
 Vergely, J. L., Ferrero, R. F., Egret, D., & Koeppen, J. 1998, *A&A*, 340, 543
 Vukotić, B., Steinhauser, D., Martínez-Aviles, G., et al. 2016, *MNRAS*, 459, 3512
 Walcher, C. J., Wisotzki, L., Bekeraité, S., et al. 2014, *A&A*, 569, A1
 Wall, J. V. & Jenkins, C. R. 2003, *Practical Statistics for Astronomers*, Cambridge Observing Handbooks for Research Astronomers (Cambridge University Press)
 Whitten, D. D., Placco, V. M., Beers, T. C., et al. 2021, *ApJ*, 912, 147
 Yan, R., Chen, Y., Lazarz, D., et al. 2019, *ApJ*, 883, 175
 Yanny, B., Rockosi, C., Newberg, H. J., et al. 2009, *AJ*, 137, 4377
 Zackrisson, E., Calisendorff, P., González, J., et al. 2016, *ApJ*, 833, 214
 Zucker, C., Goodman, A. A., Alves, J., et al. 2022, *Nature*, 601, 334